ACS OMEGA

Open Access

http://pubs.acs.org/journal/acsodf

Article

Carbon Nanofibers as Supporting Substrate for Growth of Polyaniline Nanorods on Fe_2O_3 Nanoneedles toward Electrochemical Energy Storage

Yuanhang Gu,[‖] Junjie Ding,[‖] Guang Hu, Feng You, Shaoyun Chen,* Huabo Huang,* and Chenglong Hu*

Cite This: *ACS Omega* 2024, 9, 50237−50245

Read Online

ACCESS | Metrics & More | Article Recommendations | Supporting Information

ABSTRACT: Iron-oxide (Fe_2O_3) nanoneedles were first in situ grown on the surface of carbon nanofibers (CNFs) using hydrothermal and N_2 annealing process, and then polyaniline (PANI) was coated on the Fe_2O_3 nanoneedles to form network-like nanorods through dilute solution polymerization. The PANI/Fe_2O_3/CNFs binder-free electrode exhibited a high specific capacitance of 603 F/g at 1 A/g with good rate capability. (The capacitance loss was about 48.3% when the current density increased from 1.0 to 5.0 A/g.) It was caused by the fact that the PANI/Fe_2O_3/CNFs with a well-connected structure could provide a continuous electron transport path and improve the conductivity of the entire electrode. The solid-state hybrid PANI/Fe_2O_3/CNFs||PANI/Fe_2O_3/CNFs symmetric device also achieved a high energy density of 29.85 Wh/kg at a power density of 500 W/kg. This universal compatible synthetic method for the PANI/Fe_2O_3/CNFs electrode could extend to other supercapacitor electrode systems, making it easy to fabricate various ternary electrodes for supercapacitors.

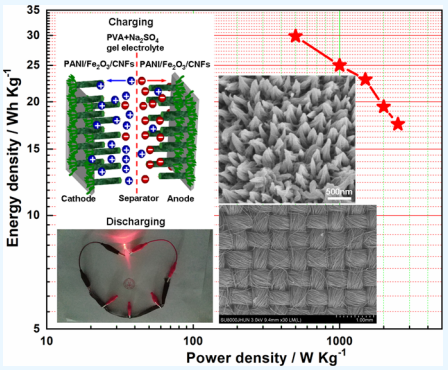

1. INTRODUCTION

Supercapacitors have high power density, outstanding rate performance, stable and long-lasting cycle life, low cost, and good safety and can be highly regarded as the next generation of energy-storage devices.[1−5] Compared with lithium-ion batteries, the commercial applications of supercapacitors are limited due to their lower energy density. However, the performance of supercapacitors, including energy density, mainly depends on the type and structure of electrode materials.[6−9] Materials that can be used as electrodes for supercapacitors contain carbon materials, such as graphene,[10] carbon nanotubes,[11] mesoporous carbon,[12,13] carbon fibers,[14,15] activated carbon,[16,17] etc., metal oxides such as MnO_2,[18] TiO_2,[19] Fe_2O_3,[20] Co_3O_4,[21] V_2O_5,[22] RuO_2,[23] etc., and conductive polymers such as polyaniline (PANI)[24,25] and polypyrrole (PPy).[26,27] However, many limitations are also exposed when the single-component material is used as an electrode. For example, carbon materials can only insert/detach a certain amount of ions during the charge/discharge process, resulting in limited energy storage and inability to meet the demand for high-density energy storage. Metal oxides have low conductivity and large volume changes, which hinder their further improvement in rate performance and cycle life. Conductive polymers are easily prone to decomposition and degradation after cycling of charge/discharge process.

Therefore, the development of composite material electrodes has become an inevitable trend, for example, binary component systems such as carbon nanotube/graphene composites,[28] graphene/metal-oxide composites,[29−31] graphene/PANI composites[32] and metal-oxide/PANI composites[33] and ternary component systems such as carbon nanotube/graphene/PANI composites,[34] graphene/PANI/MnO_2 composites,[35] graphene/PPy(PANI)/Fe_2O_3 composites,[31,36] and PANI/MnO_2/mesoporous carbon fiber composites.[37] These composite electrodes exhibit significant advantages compared with the single-component electrode: (i) Efficient energy conversion. The composite electrodes can combine the high energy-storage density and the high conductivity of active materials to achieve efficient energy conversion. (ii) High stability. The conductive materials can provide physical support to prevent the peeling of active materials in electrochemical reactions to improve the stability and lifespan of electrodes. (iii) Multifunctionality. The electrodes can be prepared for various fields such as energy storage, sensing, and electrocatalysis by selecting different active substances and conductive materials.

Received: June 19, 2024
Revised: November 28, 2024
Accepted: December 2, 2024
Published: December 13, 2024

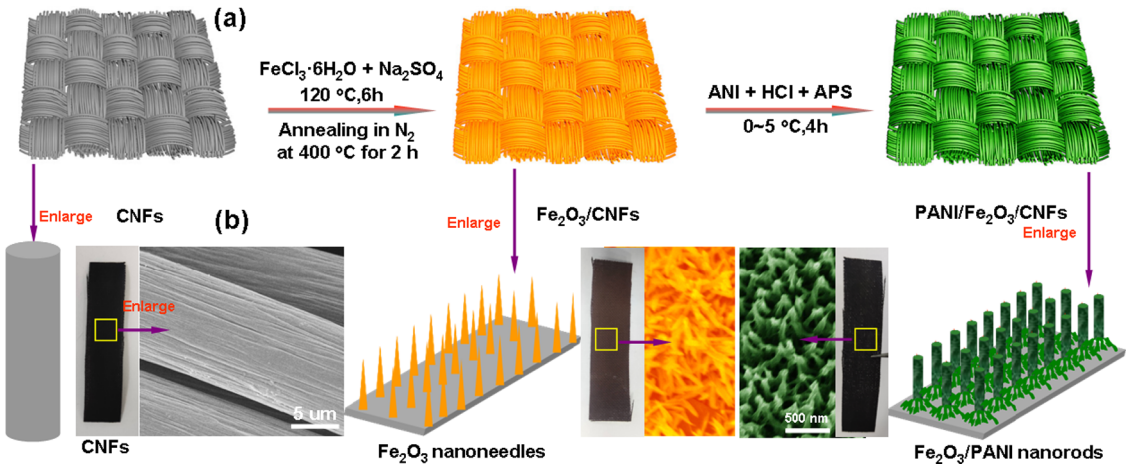

Figure 1. (a) Schematic diagram of the preparation of the PANI/Fe_2O_3/CNFs electrode. (b) Optical and SEM images of CNFs, Fe_2O_3/CNFs, and PANI/Fe_2O_3/CNFs electrode.

Based on the above discussion and our previous studies,[38−43] in this article, the iron oxide (Fe_2O_3) nanoneedles were first in situ grown onto the surface of carbon cloth fibers (CNFs) using the hydrothermal method, and then PANI nanorods grew onto the surface of Fe_2O_3 nanoneedles using dilute solution polymerization to form PANI/Fe_2O_3/CNFs ternary electrode. The CNFs as an electrode-supporting substrate have the following advantages: first, the CNFs have a large specific surface area, which can adsorb more reactive metal ions on its surface to form crystal nuclei, thereby regulating the growth and morphology of metal-oxide crystals. Second, the CNFs have good chemical stability in electrochemical reaction, which can withstand higher current densities to match various electrochemical reactions. Third, the CNFs have good physical properties, such as high strength, high hardness, and good rigidity, which can adapt to various environments. PANI is widely used as an electrode material for pseudocapacitors due to its conjugated chemical structure, unique doping phenomenon, high conductivity, and good electrochemical and environmental stabilities.[44] Fe_2O_3 is an environmentally friendly and low-cost negative potential pseudocapacitive material with a high theoretical capacitance in aqueous electrolytes. For example, Li et al. proposed a hybrid core-branch nanoarchitecture by integrating Fe_2O_3 nanoneedles on ultrafine nickel nanotube arrays, and the specific capacitance of the electrode was 418.7 F/g at 10 mV/s.[45] This article showed that the specific capacitance of Fe_2O_3/CNFs and PANI/Fe_2O_3/CNFs electrodes was 418 and 603 F/g, respectively. The capacitance retention of Fe_2O_3/CNFs was 62.4%, while that of PANI/Fe_2O_3/CNFs was 69.9% after 1000 cycles of charge−discharge, and the energy density of single PANI/Fe_2O_3/CNFs||PANI/Fe_2O_3/CNFs symmetric device is 29.85 Wh/kg at a power density of 500 W/kg.

2. EXPERIMENTAL SECTION

2.1. Materials and Equipment. CNFs were purchased from Nantong Senyou Carbon Fiber Co., Ltd. Concentrated hydrochloric acid (HCl, 37 wt %), sodium sulfate (Na_2SO_4), hexahydrate ferric chloride ($FeCl_3·6H_2O$), aniline, and ammonium persulfate ($(NH_4)_2S_2O_8$, APS) are all analytical reagents and purchased from Sinopharm Chemical Reagent Co., Ltd. Scanning electron microscopy (SEM, SU8010, Hitachi), X-ray photoelectron spectroscopy (XPS, SUPRA$^+$, Shimadzu), Raman spectrometry (Renishaw inVia), X-ray diffraction (XRD, D-MAX 2200, Panalystic), and electrochemical workstation (CHI760F, Shanghai Chenhua Co., Ltd.) were used.

2.2. Preparation of PANI/Fe_2O_3/CNFs Electrode. *2.2.1. Cleaning CNFs.* The CNFs were tailored to form a rectangular shape with 1 × 2.5 cm^2, which were successively ultrasonically cleaned with acetone, ethanol, and deionized water, and then they were dried under vacuum at 50 °C for 2 h. The weight of the CNFs is m_o (g).

2.2.2. Preparation of Fe_2O_3/CNFs Electrode. 3.5 mmol $FeCl_3·6H_2O$ (0.946 g) was dissolved in 30 mL of distilled water to form solution A. 3.5 mmol Na_2SO_4 (0.497 g) was dissolved in 10 mL of distilled water to form solution B. Solutions A and B were mixed by magnetic stirring for 30 min to transfer into a 50 mL reaction kettle lined with polytetrafluoroethylene, and then the CNFs were immersed into the mixed solution to react at 120 °C for 6 h. The as-prepared CNFs were naturally cooled at room temperature and rinsed with distilled water four to five times to dry at 60 °C for 6 h. Finally, the dried CNFs were annealed in a tube furnace for 2 h at 400 °C by N_2. After cooling to room temperature, the mass of Fe_2O_3/CNFs electrode is $m_1(g)$, and that of Fe_2O_3 loaded on CNFs is $m_1 - m_o$.

2.2.3. Preparation of PANI/Fe_2O_3/CNFs Electrode. 200 μL portion of aniline monomer was added into 0.05 M HCl aqueous solution (80 mL) to slowly stir for 5 min to form solution A in an ice bath, and then the Fe_2O_3/CNFs electrode was immersed into solution A. Two grams of APS was poured into 0.05 M HCl aqueous solution (20 mL) to dissolve to form solution B in an ice bath. Solution B was quickly mixed with solution A under slow stirring for 6 h at 0−5 °C. The products were rinsed by deionized water several times to dry at 60 °C for 12 h. The mass of PANI/Fe_2O_3/CNFs electrode is m_2 (g), the mass of PANI/Fe_2O_3 loaded on CNFs is $m_2 - m_o$, and the mass of PANI loaded on Fe_2O_3 is $m_2 - m_1$.

2.3. Electrochemical Testing. *2.3.1. Electrochemical Performance Testing of Single Electrode.* Cyclic voltammetry (CV), galvanostatic charge−discharge (GCD), and electrochemical impedance spectroscopy (EIS) were performed by a three-electrode framework: platinum sheet as the counter electrode, saturated calomel electrode (SCE) as the reference electrode, and single Fe_2O_3/CNFs and PANI/Fe_2O_3/CNFs

https://doi.org/10.1021/acsomega.4c05727
ACS Omega 2024, 9, 50237−50245

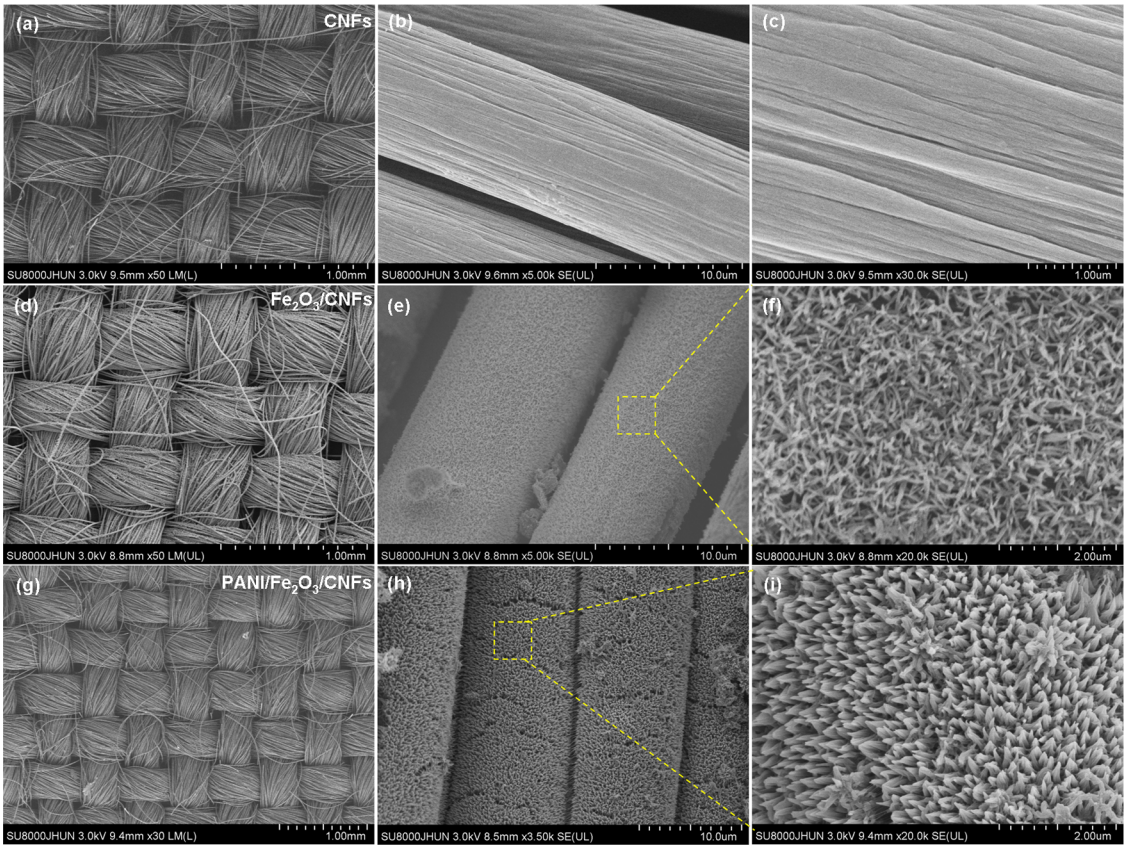

Figure 2. (a−c) SEM images of pure CNFs at different magnifications. (d−f) SEM images of Fe_2O_3/CNFs at different magnifications. (g−i) SEM images of PANI/Fe_2O_3/CNFs at different magnifications.

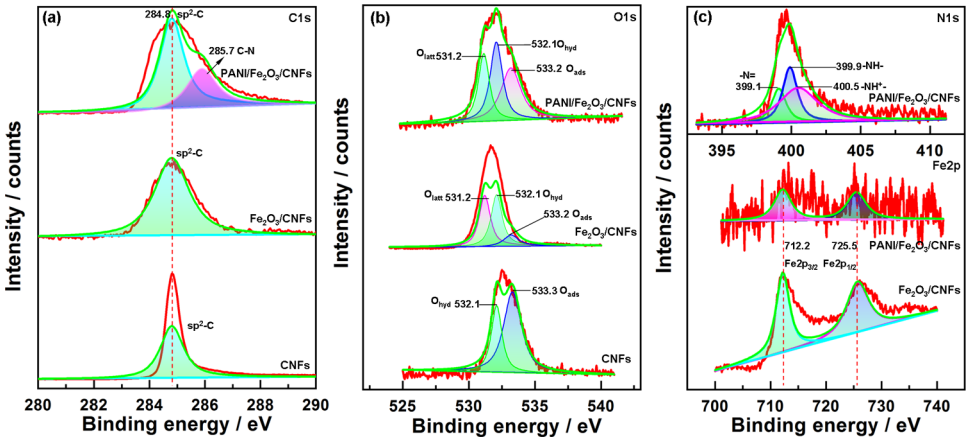

Figure 3. High-resolution spectra of C 1s (a), O 1s (b), and Fe 2p and N 1s (c) in CNFs, Fe_2O_3/CNFs, and PANI/Fe_2O_3/CNFs.

electrode as the working electrode. The voltage windows of CV and GCD curves were −1−0 V. The frequency of the EIS curve was 0.01−100 kHz. The electrolyte solution is 1 mol/L Na_2SO_4 aqueous solution.

2.3.2. Electrochemical Performance Testing of the Device. The two pieces of PANI/Fe_2O_3/CNFs electrodes and one filter paper (as a separator) were immersed into Na_2SO_4 solution (1 mol/L) for 24 h, and then the PANI/Fe_2O_3/CNFs||filter paper||PANI/Fe_2O_3/CNFs symmetric device was prepared. The electrochemical performances of the single device and multiple series device were carried out by a two-electrode framework, and the voltage window was −0.2−0.8 V.

3. RESULTS AND DISCUSSION

The preparation of the PANI/Fe_2O_3/CNFs electrode is shown in Figure 1. First, the Fe_2O_3 nanoneedles are in situ grown onto the surface of CNFs using a two-step reaction including hydrothermal and annealing process to form Fe_2O_3/CNFs electrode. Subsequently, a dilute solution polymerization method is employed to obtain PANI nanorods on the surface of Fe_2O_3 nanoneedles, yielding the PANI/Fe_2O_3/CNFs electrode. It can be seen that the pure CNFs electrode is black, and then it turns tangerine after the growth of the Fe_2O_3 nanoneedles, as shown in Figure 1a. Finally, the outer surface of Fe_2O_3 is uniformly coated with a layer of PANI to form a dark green electrode, as shown in Figure 1b. Therefore, it can

https://doi.org/10.1021/acsomega.4c05727
ACS Omega 2024, 9, 50237−50245

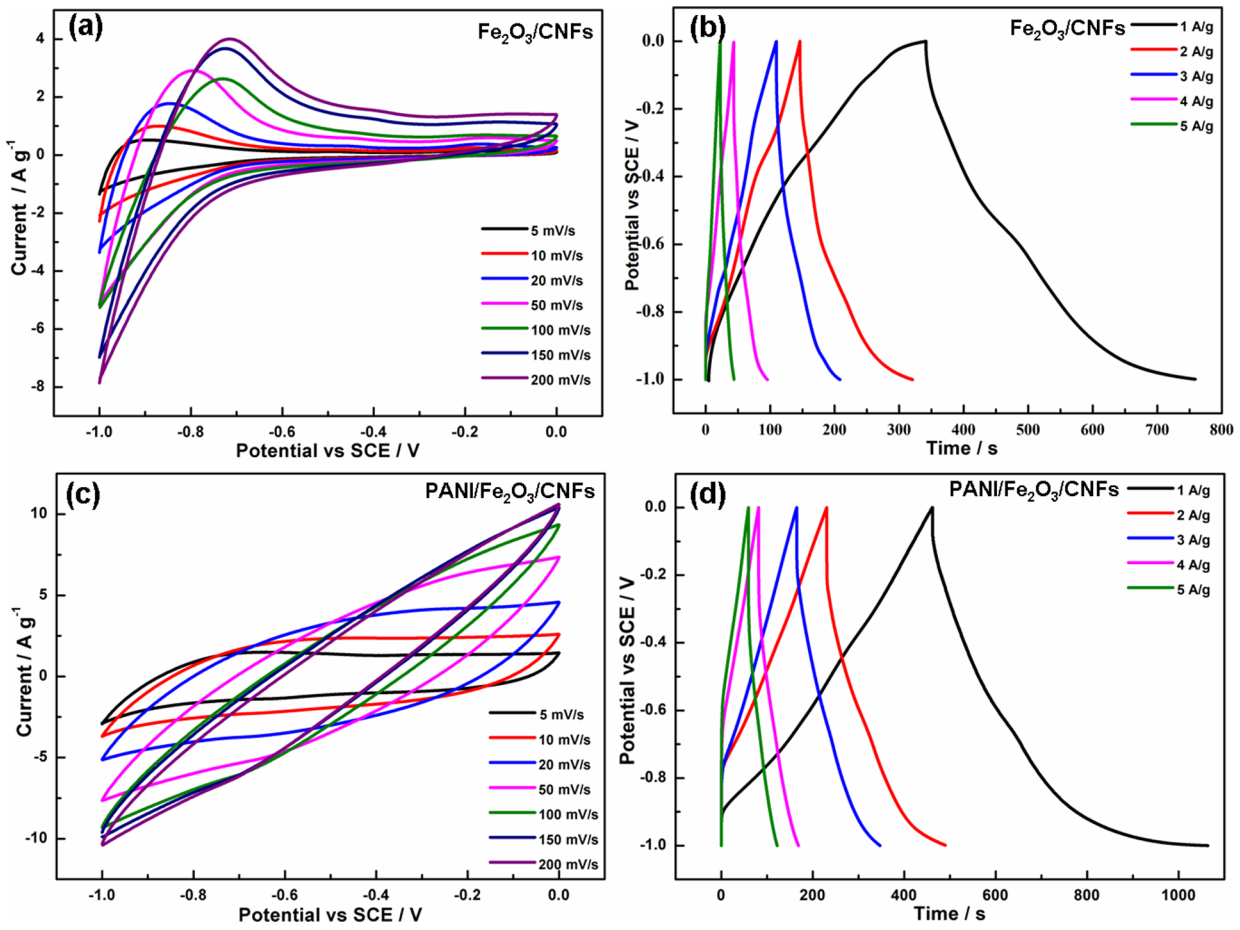

Figure 4. CV (a) and GCD (b) curves of the Fe_2O_3/CNFs electrode at different scan rates and current densities. CV (c) and GCD (d) curves of PANI/Fe_2O_3/CNFs electrode at different scan rates and current densities.

be inferred that the expected products are successfully prepared according to color change.

The CNFs with good mechanical stability can be directly used as an electrode-supporting substrate. The carbon cloth is composed of numerous carbon fibers by interweaving in a regular manner (Figure 2a), and the surface of the carbon fiber is very smooth and clean with no other interfering substances loaded on its surface, as shown in Figure 2b,c. This structure provides a favorable environment for the in situ growth of Fe_2O_3. At low magnification, the appearance of the carbon cloth loaded with Fe_2O_3 nanoneedles has no significant change in comparison with pure carbon cloth, as shown in Figure 2a. However, the high-density Fe_2O_3 nanoneedles with a diameter of 40−70 nm are grown in situ on the surface of each carbon fiber, as shown in Figure 2e,f. Aniline molecules can be adsorbed to the surface of Fe_2O_3 nanoneedles through hydrogen binding to polymerize to form PANI/Fe_2O_3 nanorods with a porous network structure, and the diameter of PANI/Fe_2O_3 is about 60−100 nm, which is bigger than that of Fe_2O_3 nanoneedles, as shown in Figure 2g−i. The PANI/Fe_2O_3/CNFs with a well-connected porous structure can provide a continuous electron transport path and improve the conductivity of the entire electrode.[46] Moreover, the PANI layer fully coated on the surface of Fe_2O_3 nanoneedles can alleviate the volume expansion during the charge−discharge process. Therefore, it is expected to improve the rate performance and cycling life of the electrode.

The Raman spectra and XRD curves of CNFs, Fe_2O_3/CNFs, and PANI/Fe_2O_3/CNFs are shown in Figure S1. The survey XPS spectra of CNFs, Fe_2O_3/CNFs, and PANI/Fe_2O_3/CNFs are shown in Figures S2 and 3. The fine XPS spectra of C 1s located at 284.8 eV in all samples are related to sp^2 of C−C, and the binding energy located at 285.7 eV is assigned to the C−N in the PANI macromolecular chain, as shown in Figure 3a. The fine XPS spectra of O 1s in CNFs can be fitted into two components at binding energies of 532.1 eV (O_{hyd}) and 533.3 eV (O_{ads}). For the Fe_2O_3/CNFs, the binding energy located at 531.2 eV originates from the O_{latt} of the Fe−O, as shown in Figure 3b. The binding energy located at 712.2 and 725.5 eV is assigned to Fe $2p_{3/2}$ and Fe $2p_{1/2}$, respectively, and the spin energy separation of two peaks is 13.3 eV, in agreement with the reported value of α-Fe_2O_3,[47] as shown in the bottom of Figure 3c. For PANI/Fe_2O_3/CNFs, the peaks located at 399.1, 399.9, and 400.5 eV is related to −N= in quinoid, −NH− in amide groups, and $-NH^+-$ in emeraldine salt,[48] respectively, as shown in the top of Figure 3c. The results indicate that PANI has successfully grown on the surface of Fe_2O_3 without damaging the crystal structure of Fe_2O_3.

The CV curves of the CNFs, Fe_2O_3/CNFs, and PANI/Fe_2O_3/CNFs electrodes are shown in Figure S3. It can be seen that the order of the area of CV Curve is PANI/Fe_2O_3/CNFs> Fe_2O_3/CNFs > CNFs, indicating that the PANI/Fe_2O_3/CNFs electrode has good electrochemical response. The CV curves of the Fe_2O_3/CNFs electrodes at different scan rates are shown

https://doi.org/10.1021/acsomega.4c05727
ACS Omega 2024, 9, 50237−50245

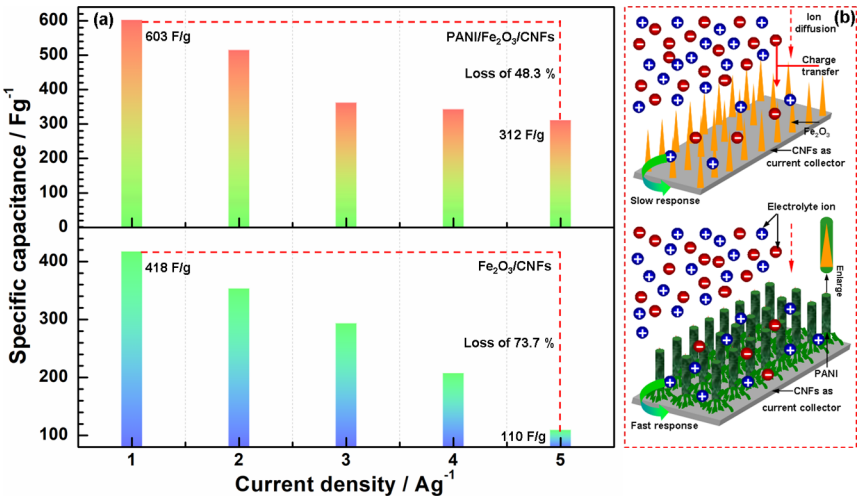

Figure 5. (a) Relationship between specific capacitance and current density. (b) Possible migration mechanism of electrolyte ions in Fe_2O_3/CNFs and PANI/Fe_2O_3/CNFs electrodes.

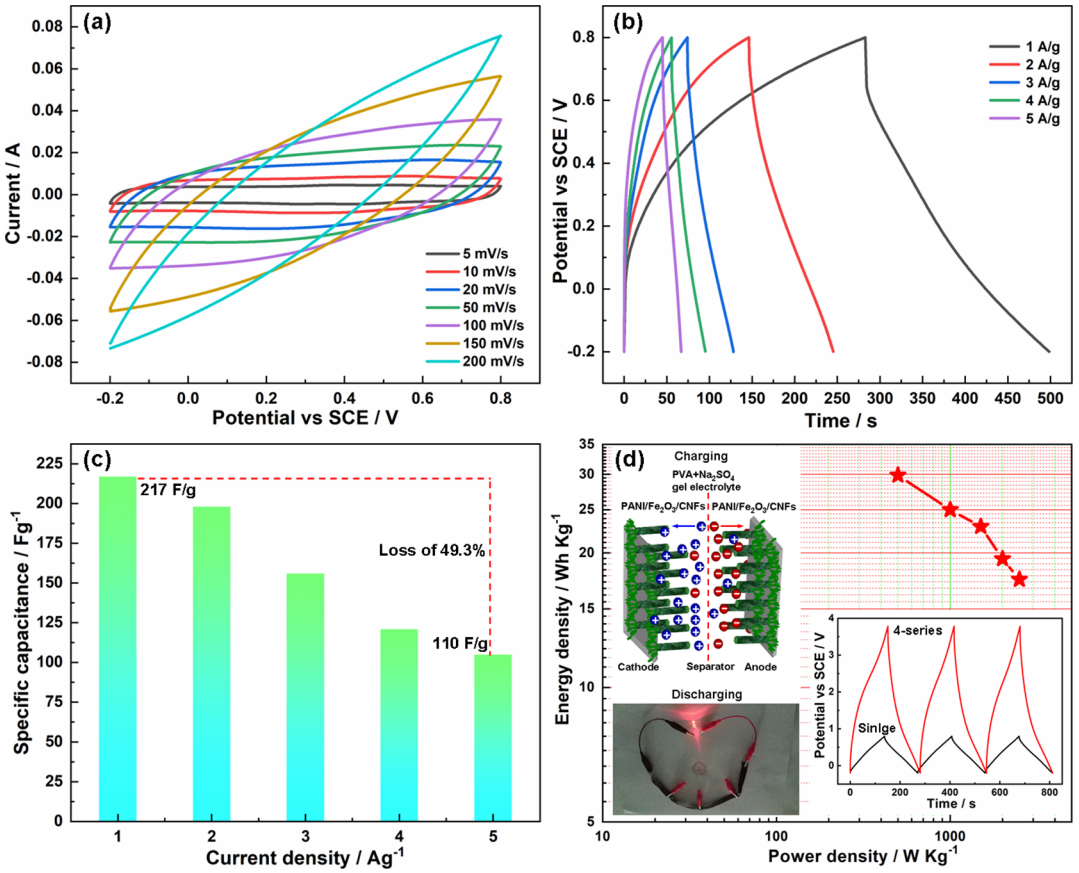

Figure 6. CV (a) and GCD (b) curves of the PANI/Fe_2O_3/CNFs||PANI/Fe_2O_3/CNFs symmetric device at different scan rates and current densities, respectively. (c) Relationship between the current density and specific capacitance. (d) Ragone plots of the PANI/Fe_2O_3/CNFs||PANI/Fe_2O_3/CNFs symmetric device. Top inset is the possible migration mechanism of electrolyte ions. Bottom inset is a photograph of the red LED driven by the four-series tandem device. The GCD curves of single and 4-series device are shown at the bottom right.

in Figure 4a. It can be seen that the oxidation peak of the Fe_2O_3/CNFs electrode shifts toward the positive along with the increase of scan rates due to the electrochemical polarization in the Faraday reaction.[49] The GCD curves of the Fe_2O_3/CNFs electrode at different current densities are shown in Figure 4b. All of the charge−discharge curves are nearly symmetric triangular curves, indicating that the Fe_2O_3 nanoneedles adsorb Na^+ to participate in the electrode reaction, and the specific capacitance decreases with the increase of current density. The specific capacitance can be calculated by the following eq 1:[38]

$$SC = \frac{I \times \triangle t}{V \times m} \quad (1)$$

https://doi.org/10.1021/acsomega.4c05727
ACS Omega 2024, 9, 50237−50245

The specific capacitance of the Fe_2O_3/CNFs electrode is about 418 F/g at 1 A/g. The CV curves of the PANI/Fe_2O_3/CNFs electrode at different scan rates are shown in Figure 4c. At low scan rate, a pair of redox peaks of the CV curve can be found, which relates with the structural transformation between leucoemeraldine and emeraldine in PANI.[50] It was also found that the CV curves of the PANI/Fe_2O_3/CNFs electrode can keep the same shape at low scan rates (5−50 mV/s), indicating that the PANI/Fe_2O_3/CNFs electrode has low resistance for charge transfer and electrolyte ion diffusion. However, the redox peak of the CV curve disappears when the scan rate is increased from 100 to 200 mV/s. It is attributed to the electrochemical and concentration polarization at high scan speeds, leading to a decrease in the utilization of active materials. The GCD curves of the PANI/Fe_2O_3/CNFs electrode at different current densities are shown in Figure 4d, and the specific capacitance of the PANI/Fe_2O_3/CNFs electrode is about 603 F/g at 1 A/g, which is much higher than that of the Fe_2O_3/CNFs electrode. The comparison between the PANI/Fe_2O_3/CNFs electrode and the recently reported Fe_2O_3 and Fe_2O_3-based electrodes is shown in Table S1. It is found that the specific capacitance of the PANI/Fe_2O_3/CNFs electrode is superior or close to individual Fe_2O_3 and Fe_2O_3-based electrodes. The PANI nanorods can form a cross-linked network structure after growth onto the surface of Fe_2O_3 nanoneedles, and then the each PANI/Fe_2O_3/CNFs acts as a continuous conductive to reduce the interface resistance of components and improve the charge transfer and ion diffusion rate to enhance the electrochemical performance. In addition, the capacitive and diffusion contributions in the PANI/Fe_2O_3/CNFs electrode can be found in Figure S4.

The relationship between the specific capacitance and current density is shown in Figure 5a. The capacitance loss of the Fe_2O_3/CNFs electrode is about 73.3%, while that of the PANI/Fe_2O_3/CNFs electrode is about 48.3% when the current density increases from 1.0 to 5.0 A/g. The possible mechanism can be seen in Figure 5b. First, the transmission and migration of electrolyte ions are limited due to the poor conductivity of Fe_2O_3. The migration rate of ions cannot keep up with the changing of current at high current density, resulting in a slow response of Faraday reaction. Second, the specific capacitance and rate performance of the PANI/Fe_2O_3/CNFs electrode are greatly improved when PANI grows on the surface of Fe_2O_3 nanoneedles. It is attributed to the fact that the acid-doped PANI with good conductivity can accelerate the transport and migration of electrolyte ions. In addition, the PANI nanorods coated on Fe_2O_3 can greatly reduce the interface contact resistance to further accelerate the conduction of ions, resulting in fast response of Faraday reaction to improve the rate performance.

In order to explore the practical application of the PANI/Fe_2O_3/CNFs electrode, the symmetric supercapacitor device is assembled by a sandwich structure. Figure 6a shows the CV curves of the symmetric device at different scanning rates. It can be seen that all CV curves with high symmetry are quasi rectangular, revealing good reversibility and typical capacitive behavior. Moreover, the shape of the CV curve is well preserved at 200 mV/s, indicating that the symmetric device has good rate performance. The GCD curves of the symmetric device have no IR-drop at different current densities, indicating the low internal resistance present in the PANI/Fe_2O_3/CNFs electrode, as shown in Figure 6b.[45] The power density and energy density of a single symmetric device are calculated from Figure 6c, as shown in Figure 6d. The maximum energy density of 29.85 Wh/kg is obtained at the power density of 500 W/kg, which is much higher or close to our previous studies and latest reports, such as pure PANI nanorods/CNFs (10.04 Wh/kg at 225 W/kg),[38] PANI nanorod/graphite flake (18.75 Wh/kg at 500 W/kg),[39] oxygen vacancy-Fe_2O_3@PANI@CNFs (12.125 Wh/kg at 250 W/kg),[46] Fe_2O_3/PANI (11.28 Wh/kg at 162 W/kg),[51] and $NiCo_2O_4$/NiO‖Fe_2O_3-based device (19 Wh/kg at 157 W/kg).[52] The process of charging related to the transport and migration of electrolyte ions of the PANI/Fe_2O_3/CNFs‖PANI/Fe_2O_3/CNFs symmetric device is shown in the top inset of Figure 6d, and the red light-emitting diode (LED, 1.8−3.5 V) can be lit up when four single devices are connected in series. It can be explained that the working voltage range of a single device is −0.2 to 0.8 V, and four devices connected in series can achieve a working voltage of 4.0 V (at the bottom right of the Figure 6d), ensuring that the LED is lit up in a normal way, as shown in the bottom inset of Figure 6d.

The capacitance retention of specific capacitance of the Fe_2O_3/CNFs and PANI/Fe_2O_3/CNFs electrodes at 10 A/g is shown in Figure 7. It can be seen that the capacitance retention

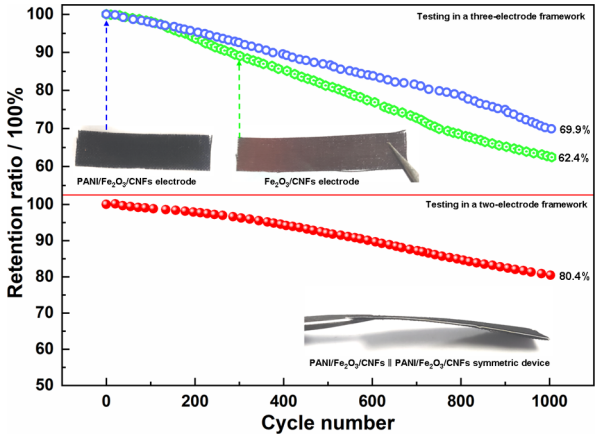

Figure 7. Cyclic stability of the Fe_2O_3/CNFs electrode, PANI/Fe_2O_3/CNFs electrode, and PANI/Fe_2O_3/CNFs‖PANI/Fe_2O_3/CNFs symmetric device at 10 A/g.

of the Fe_2O_3/CNFs and PANI/Fe_2O_3/CNFs electrodes is about 62.4% and 69.9% after 1000 cycles, respectively, indicating that the synergistic effect between Fe_2O_3 and PANI can effectively improve the cycling stability. The enhanced cycling stability of the PANI/Fe_2O_3/CNFs electrode may be related to the network-like nanorods of PANI, which has a strong adhesive force between the supporting substrate (CNFs) and active materials. PANI coated on the surface of Fe_2O_3 nanoneedles can effectively prevent the collapse or separation of the structure and provide a relaxed space to adapt to the volume change of Fe_2O_3 during the charge/discharge process. Furthermore, the capacitance retention of the PANI/Fe_2O_3/CNFs‖PANI/Fe_2O_3/CNFs symmetric device is about 80.4%, which is higher than that of the PANI/Fe_2O_3/CNFs electrode. It indicates that the stability of the device is better than that of a single electrode due to the different working conditions during the charge/discharge process. In addition, the EIS curves of the Fe_2O_3/CNFs and PANI/Fe_2O_3/CNFs electrodes can be found in Figure S5. The discharge/charge efficiency of the PANI/Fe_2O_3/CNFs electrode and PANI/

https://doi.org/10.1021/acsomega.4c05727
ACS Omega 2024, 9, 50237−50245

Fe_2O_3/CNFs||PANI/Fe_2O_3/CNFs symmetric device at different current densities can be found in Figure S6.

4. CONCLUSIONS

In conclusion, the Fe_2O_3 nanoneedles were successfully in situ grown on the surface of CNFs using a chemical synthesis method, and then the network-like nanorod framework of PANI was grown on the surface of the Fe_2O_3 nanoneedles using dilute solution polymerization to obtain PANI/Fe_2O_3/CNFs electrode. The results showed that the specific capacitance of the PANI/Fe_2O_3/CNFs electrode was about 601 F/g at 1.0 A/g, which is 1.4 times than that of the Fe_2O_3/CNFs electrode. The capacitance loss of the Fe_2O_3/CNFs electrode was about 73.3%, while that of the PANI/Fe_2O_3/CNFs electrode was about 48.3%, indicating that the PANI/Fe_2O_3/CNFs electrode had good rate performance. It is due to the fact that acid-doped PANI with good conductivity could accelerate the transport and migration of electrolyte ions, reducing the interface contact resistance to accelerate conduction of ions to improve the rate performance of the electrode materials. The PANI/Fe_2O_3/CNFs||PANI/Fe_2O_3/CNFs symmetric device was also assembled by a sandwich structure, and the maximum energy density was 29.85 Wh/kg at the power density of 500 W/kg, which was much higher than or close to our previous studies and latest reports.

■ ASSOCIATED CONTENT

Supporting Information

The Supporting Information is available free of charge at https://pubs.acs.org/doi/10.1021/acsomega.4c05727.

Raman spectra and XRD curves of CNFs, Fe_2O_3/CNFs, and PANI/Fe_2O_3/CNFs electrode; survey XPS spectra of the CNFs, Fe_2O_3/CNFs and PANI/Fe_2O_3/CNFs; CV and GCD curves of the CNFs, Fe_2O_3/CNFs and PANI/Fe_2O_3/CNFs electrodes; linear plots; EIS curves; discharge-charge efficiency of the PANI/Fe_2O_3/CNFs electrode and PANI/Fe_2O_3/CNFs||PANI/Fe_2O_3/CNFs symmetric device at different current densities; and comparison of specific capacitance between the PANI/Fe_2O_3/CNFs electrode and the recently reported Fe_2O_3-based electrodes (PDF)

■ AUTHOR INFORMATION

Corresponding Authors

Shaoyun Chen − *School of Optoelectronic Materials & Technology, Jianghan University, Wuhan 430056, China*; Email: cescsy@jhun.edu.cn

Huabo Huang − *Hubei Key Laboratory of Plasma Chemistry and Advanced Materials, Key Laboratory for Green Chemical Process of Ministry of Education, School of Materials Science and Engineering, Wuhan Institute of Technology, Wuhan 430205, China*; orcid.org/0000-0001-5545-5916; Email: hbhuang@wit.edu.cn

Chenglong Hu − *School of Optoelectronic Materials & Technology, Jianghan University, Wuhan 430056, China*; orcid.org/0000-0003-1554-269X; Email: ceshcl@jhun.edu.cn

Authors

Yuanhang Gu − *School of Optoelectronic Materials & Technology, Jianghan University, Wuhan 430056, China; Hubei Key Laboratory of Plasma Chemistry and Advanced Materials, Key Laboratory for Green Chemical Process of Ministry of Education, School of Materials Science and Engineering, Wuhan Institute of Technology, Wuhan 430205, China*

Junjie Ding − *Wuhan Lvzhixing Technology Co., Ltd, Wuhan 430206, China*

Guang Hu − *School of Optoelectronic Materials & Technology, Jianghan University, Wuhan 430056, China*

Feng You − *Hubei Key Laboratory of Plasma Chemistry and Advanced Materials, Key Laboratory for Green Chemical Process of Ministry of Education, School of Materials Science and Engineering, Wuhan Institute of Technology, Wuhan 430205, China*

Complete contact information is available at: https://pubs.acs.org/10.1021/acsomega.4c05727

Author Contributions

‖Y.G. and J.D. contributed equally to this work.

Notes

The authors declare no competing financial interest.

■ ACKNOWLEDGMENTS

This work was supported by the Natural Science Foundation of Hubei Province (2023AFB890 and 2021CFB507) and the Open Project of State Key Laboratory of Advanced Technology for Materials Synthesis and Processing (Wuhan University of Technology) (2022-KF-18).

■ REFERENCES

(1) Zhu, Q.; Zhao, D.; Cheng, M.; Zhou, J.; Owusu, K. A.; Mai, L.; Yu, Y. A new view of supercapacitors: integrated supercapacitors. *Adv. Energy Mater.* **2019**, *9*, No. 901081.

(2) Zhao, J.; Burke, A. F. Review on supercapacitors: Technologies and performance evaluation. *J. Energy Chem.* **2021**, *59*, 276−291.

(3) Sharma, P.; Kumar, V. Current technology of supercapacitors: A review. *J. Electron. Mater.* **2020**, *49*, 3520−3532.

(4) Poonam; Sharma, K.; Arora, A.; Tripathi, S. K. Review of supercapacitors: Materials and devices. *J. Energy Storage* **2019**, *21*, 801−825.

(5) Olabi, A. G.; Abbas, Q. A.; Makky, Al.; Abdelkareem, M. A. Supercapacitors as next generation energy storage devices: Properties and applications. *Energy* **2022**, *248*, No. 123617.

(6) Forouzandeh, P.; Kumaravel, V.; Pillai, S. C. Electrode materials for supercapacitors: a review of recent advances. *Catalysts* **2020**, *10*, 969.

(7) Liang, B.; Du, Y.; Xiao, P.; Cheng, J.; Yuan, S.; Chen, Y.; Yuan, J.; Chen, J. Transition metal oxide electrode materials for supercapacitors: a review of recent developments. *Nanomaterials* **2021**, *11*, 1248.

(8) Wang, G.; Zhang, L.; Zhang, J. A review of electrode materials for electrochemical supercapacitors. *Chem. Soc. Rev.* **2012**, *41*, 797−828.

(9) Wang, F.; Wu, X.; Yuan, X.; Liu, Z.; Zhang, Y.; Fu, L.; Zhu, Y.; Zhou, Q.; Wu, Y.; Huang, W. Latest advances in supercapacitors: from new electrode materials to novel device designs. *Chem. Soc. Rev.* **2017**, *46*, 6816−6854.

(10) Velasco, A.; Ryu, Y. K.; Boscá, A.; Ladrón-de-Guevara, A.; Hunt, E.; Zuo, J.; Pedrós, J.; Calle, F.; Martinez, J. Recent trends in graphene supercapacitors: from large area to microsupercapacitors. *Sustain. Energy Fuels* **2021**, *5*, 1235−1254.

(11) Zhu, S.; Ni, J.; Li, Y. Carbon nanotube-based electrodes for flexible supercapacitors. *Nano Res.* **2020**, *13*, 1825−1841.

(12) Bairi, P.; Maji, S.; Hill, J. P.; Kim, J. H.; Ariga, K.; Shrestha, L. K. Mesoporous carbon cubes derived from fullerene crystals as a high

rate performance electrode material for supercapacitors. *J. Mater. Chem. A* **2019**, *7*, 12654−12660.
(13) Qiu, Y.; Hou, M.; Gao, J.; Zhai, H.; Liu, H.; Jin, M.; Liu, X.; Lai, L. One-step synthesis of monodispersed mesoporous carbon nanospheres for high-performance flexible quasi-solid-state micro-supercapacitors. *Small* **2019**, *15*, No. 1903836.
(14) Ma, C.; Wu, L.; Dirican, M.; Cheng, H.; Li, J.; Song, Y.; Shi, J.; Zhang, X. Carbon black-based porous sub-micron carbon fibers for flexible supercapacitors. *Appl. Surf. Sci.* **2021**, *537*, No. 147914.
(15) Shi, L.; Ye, J.; Lu, H.; Wang, G.; Lv, J.; Ning, G. Flexible all-solid-state supercapacitors based on boron and nitrogen-doped carbon network anchored on carbon fiber cloth. *Chem. Eng. J.* **2021**, *410*, No. 128365.
(16) Sundriyal, S.; Shrivastav, V.; Pham, H. D.; Mishra, S.; Deep, A.; Dubal, D. P. Advances in bio-waste derived activated carbon for supercapacitors: Trends, challenges and prospective. *Resour. Conserv. Recy.* **2021**, *169*, No. 105548.
(17) Reis, G. S. D.; Larsson, S. H.; de Oliveira, H. P.; Thyrel, M.; Lima, E. C. Sustainable biomass activated carbons as electrodes for battery and supercapacitors-A mini-review. *Nanomaterials* **2020**, *10*, 1398.
(18) Guo, W.; Yu, C.; Li, S.; Wang, Z.; Yu, J.; Huang, H.; Qiu, J. Strategies and insights towards the intrinsic capacitive properties of MnO_2 for supercapacitors: challenges and perspectives. *Nano Energy* **2019**, *57*, 459−472.
(19) Chen, S. Y.; Liu, B.; Zhang, X. Y.; Chen, F.; Shi, H.; Hu, C. L.; Chen, J. Growth of polyaniline on TiO_2 tetragonal prism arrays as electrode materials for supercapacitor. *Electrochim. Acta* **2019**, *300*, 373−379.
(20) Yu, P.; Duan, W.; Jiang, Y. Porous Fe_2O_3 nanorods on hierarchical porous biomass carbon as advanced anode for high-energy-density asymmetric supercapacitors. *Front. Chem.* **2020**, *8*, No. 611852.
(21) Wang, X.; Hu, A.; Meng, C.; Wu, C.; Yang, S.; Hong, X. Recent advance in Co_3O_4 and Co_3O_4-containing electrode materials for high-performance supercapacitors. *Molecules* **2020**, *25*, 269.
(22) Majumdar, D.; Mandal, M.; Bhattacharya, S. K. V_2O_5 and its carbon-based nanocomposites for supercapacitor applications. *Chem. Electro. Chem.* **2019**, *6*, 1623−1648.
(23) Jeon, S.; Jeong, J. H.; Yoo, H.; Yu, H. K.; Kim, B. H.; Kim, M. H. RuO_2 nanorods on electrospun carbon nanofibers for supercapacitors. *ACS Appl. Nano Mater.* **2020**, *3*, 3847−3858.
(24) Liu, P.; Yan, J.; Guang, Z.; Huang, Y.; Li, X.; Huang, W. Recent advancements of polyaniline-based nanocomposites for supercapacitors. *J. Power. Sources* **2019**, *424*, 108−130.
(25) Banerjee, J.; Dutta, K.; Kader, M. A.; Nayak, S. K. An overview on the recent developments in polyaniline-based supercapacitors. *Polym. Adv. Technol.* **2019**, *30*, 1902−1921.
(26) Shimoga, G.; Palem, R. R.; Choi, D. S.; Shin, E. J.; Ganesh, P. S.; Saratale, G. D.; Saratale, R. G.; Lee, S. H.; Kim, S. Y. Polypyrrole-based metal nanocomposite electrode materials for high-performance supercapacitors. *Metals* **2021**, *11*, 905.
(27) Huang, Y.; Li, H.; Wang, Z.; Zhu, M.; Pei, Z.; Xue, Q.; Huang, Y.; Zhi, C. Y. Nanostructured polypyrrole as a flexible electrode material of supercapacitor. *Nano Energy* **2016**, *22*, 422−438.
(28) Yang, Z.; Tian, J.; Yin, Z.; Cui, C.; Qian, W.; Wei, F. Carbon nanotube-and graphene-based nanomaterials and applications in high-voltage supercapacitor: A review. *Carbon* **2019**, *141*, 467−480.
(29) Ansarinejad, H.; Shabani-Nooshabadi, M.; Ghoreishi, S. M. Enhanced supercapacitor performance using a Co_3O_4@Co_3S_4 nanocomposite on reduced graphene oxide/Ni foam electrodes. *Chemasian J.* **2021**, *16*, 1258−1270.
(30) Wang, H.; Fu, Q.; Pan, C. Green mass synthesis of graphene oxide and its MnO_2 composite for high performance supercapacitor. *Electrochim. Acta* **2019**, *312*, 11−21.
(31) Gupta, A.; Sardana, S.; Dalal, J.; Lather, S.; Maan, A. S.; Tripathi, R.; Punia, R.; Singh, K.; Ohlan, A. Nanostructured polyaniline/graphene/Fe_2O_3 composites hydrogel as a high-performance flexible supercapacitor electrode material. *ACS Appl. Energy Mater.* **2020**, *3*, 6434−6446.
(32) Balqis, F.; Prakoso, B.; Hawari, N. H.; Eldona, C.; Sumboja, A. Recent development of polyaniline/graphene composite electrodes for flexible supercapacitor devices. *ChemNanoMat* **2022**, *8*, No. e202200151.
(33) Morshed, M.; Wang, J.; Gao, M.; Cong, C.; Wang, Z. Polyaniline and rare earth metal oxide composition: a distinctive design approach for supercapacitor. *Electrochim. Acta* **2021**, *370*, No. 137714.
(34) Wang, C.; Yang, Y.; Li, R.; Wu, D.; Qin, Y.; Kong, Y. Polyaniline functionalized reduced graphene oxide/carbon nanotube ternary nanocomposite as a supercapacitor electrode. *Chem. Commun.* **2020**, *56*, 4003−4006.
(35) Xu, A.; Yu, Y.; Li, W.; Zhang, Y.; Ye, S.; Zhao, Z.; Qin, Y. Sequential electrodeposition fabrication of graphene/polyaniline/MnO_2 ternary supercapacitor electrodes with high rate capability and cyclic stability. *Electrochim. Acta* **2022**, *435*, No. 141378.
(36) Vigneshwaran, J.; Abraham, S.; Muniyandi, B.; Prasankumar, T.; Li, J. T.; Jose, S. Fe_2O_3 decorated graphene oxide/polypyrrole matrix for high energy density flexible supercapacitor. *Surf. Interfaces* **2021**, *227*, No. 101572.
(37) Dirican, M.; Yanilmaz, M.; Asiri, A. M.; Zhang, X. Polyaniline/MnO_2/porous carbon nanofiber electrodes for supercapacitors. *J. Electroanal. Chem.* **2020**, *861*, No. 113995.
(38) Hu, C. L.; Zhang, X. Y.; Liu, B.; Chen, S. Y.; Liu, X. Q.; Liu, Y. M.; Liu, J. Y.; Chen, J. Orderly and highly dense polyaniline nanorod arrays fenced on carbon nanofibers for all-solid-state flexible electrochemical energy storage. *Electrochim. Acta* **2020**, *338*, No. 135846.
(39) Liu, B.; Zhang, X. Y.; Tian, D.; Li, Q.; Zhong, M.; Chen, S. Y.; Hu, C. L.; Ji, H. B. In situ growth of oriented polyaniline nanorod arrays on the graphite flake for high-performance supercapacitors. *ACS omega* **2020**, *5*, 32395−32402.
(40) Peng, S.; Liu, B.; Zhang, X. Y.; Li, W. H.; Chen, S. Y.; Hu, C. L.; Liu, X. Q.; Liu, J. Y.; Chen, J. Large-area polyaniline nanorod growth on a monolayer polystyrene nanosphere array as an electrode material for supercapacitors. *ACS Appl. Energy Mater.* **2021**, *4*, 14766−14777.
(41) Tian, D.; Cheng, H.; Li, Q.; Song, C.; Wu, D.; Zhao, X. Y.; Hu, S. Q.; Chen, S. Y.; Hu, C. L. The ordered polyaniline nanowires wrapped on the polypyrrole nanotubes as electrode materials for electrochemical energy storage. *Electrochim. Acta* **2021**, *398*, No. 139328.
(42) Chen, S. Y.; Zhang, Y.; Tian, D.; You, Q. L.; Zhong, M.; Hu, C. L.; Chen, J. Polyaniline combining with ultrathin manganese dioxide nanosheets on carbon nanofibers as effective binder-free supercapacitor electrode. *Electrochim. Acta* **2023**, *450*, No. 142275.
(43) Wang, Y.; Xu, S. Q.; Cheng, H.; Liu, W. F.; Chen, F.; Liu, X. Q.; Liu, J. Y.; Chen, S. Y.; Hu, C. L. Oriented growth of polyaniline nanofiber arrays onto the glass and flexible substrates using a facile method. *Appl. Surf. Sci.* **2018**, *428*, 315−321.
(44) Kuila, B. K.; Nandan, B.; Böhme, M.; Janke, A.; Stamm, M. Vertically oriented arrays of polyaniline nanorods and their super electrochemical properties. *Chem. Commun.* **2009**, *38*, 5749−5751.
(45) Li, Y.; Xu, J.; Feng, T.; Yao, F. Q.; Xie, J. P.; Xia, H. Fe_2O_3 nanoneedles on ultrafine nickel nanotube arrays as efficient anode for high-performance asymmetric supercapacitors. *Adv. Funct. Mater.* **2017**, *27*, No. 1606728.
(46) Dong, K.; Yang, Z.; Chen, J.; Shi, D.; Chen, M. Oxygen vacancy-Fe_2O_3@ polyaniline composites directly grown on carbon cloth as a high stable electrode for symmetric supercapacitors. *J. Inorg. Organomet. Poly. Mater.* **2021**, *31*, 3894−3903.
(47) Yang, X.; Sun, H.; Zhang, L.; Zhao, L.; Lian, J.; Jiang, Q. High efficient photo-Fenton catalyst of α-Fe_2O_3/MoS_2 hierarchical nano-heterostructures: reutilization for supercapacitors. *Sci. Rep.* **2016**, *6*, 31591.
(48) Lu, X. F.; Chen, X. Y.; Zhou, W. Y.; Tong, X.; Li, G. R. α-Fe_2O_3@ PANI core−shell nanowire arrays as negative electrodes for

https://doi.org/10.1021/acsomega.4c05727
ACS Omega 2024, 9, 50237−50245

asymmetric supercapacitors. *ACS Appl. Mater. Interface* **2015**, *7*, 14843−14850.
(49) Tang, Q.; Wang, W.; Wang, G. The perfect matching between the low-cost Fe_2O_3 nanowire anode and the NiO nanoflake cathode significantly enhances the energy density of asymmetric supercapacitors. *J. Mater. Chem. A* **2015**, *3*, 6662−6670.
(50) Li, G. R.; Feng, Z. P.; Zhong, J. H.; Wang, Z. L.; Tong, Y. X. Electrochemical synthesis of polyaniline nanobelts with predominant electrochemical performances. *Macromolecules* **2010**, *43*, 2178−2183.
(51) Atram, R. R.; Bhuse, D. V.; Bhuse, V. M.; Atram, R. G.; Kondawar, S. B. Evolution of waste iron rust into α-Fe_2O_3/CNF and α-Fe_2O_3/PANI composites as an efficient positive electrode for sustainable hybrid supercapacitor. *J. Mater. Sci. Mater. Electron.* **2021**, *32*, 13787−13802.
(52) Shanmugavani, A.; Selvan, R. K. Microwave assisted reflux synthesis of $NiCo_2O_4$/NiO composite: fabrication of high performance asymmetric supercapacitor with Fe_2O_3. *Electrochim. Acta* **2016**, *189*, 283−294.

https://doi.org/10.1021/acsomega.4c05727
ACS Omega 2024, 9, 50237−50245